iScience

CellPress
OPEN ACCESS

Article

Promising and efficient lignin degradation versatile strategy based on DFT calculations

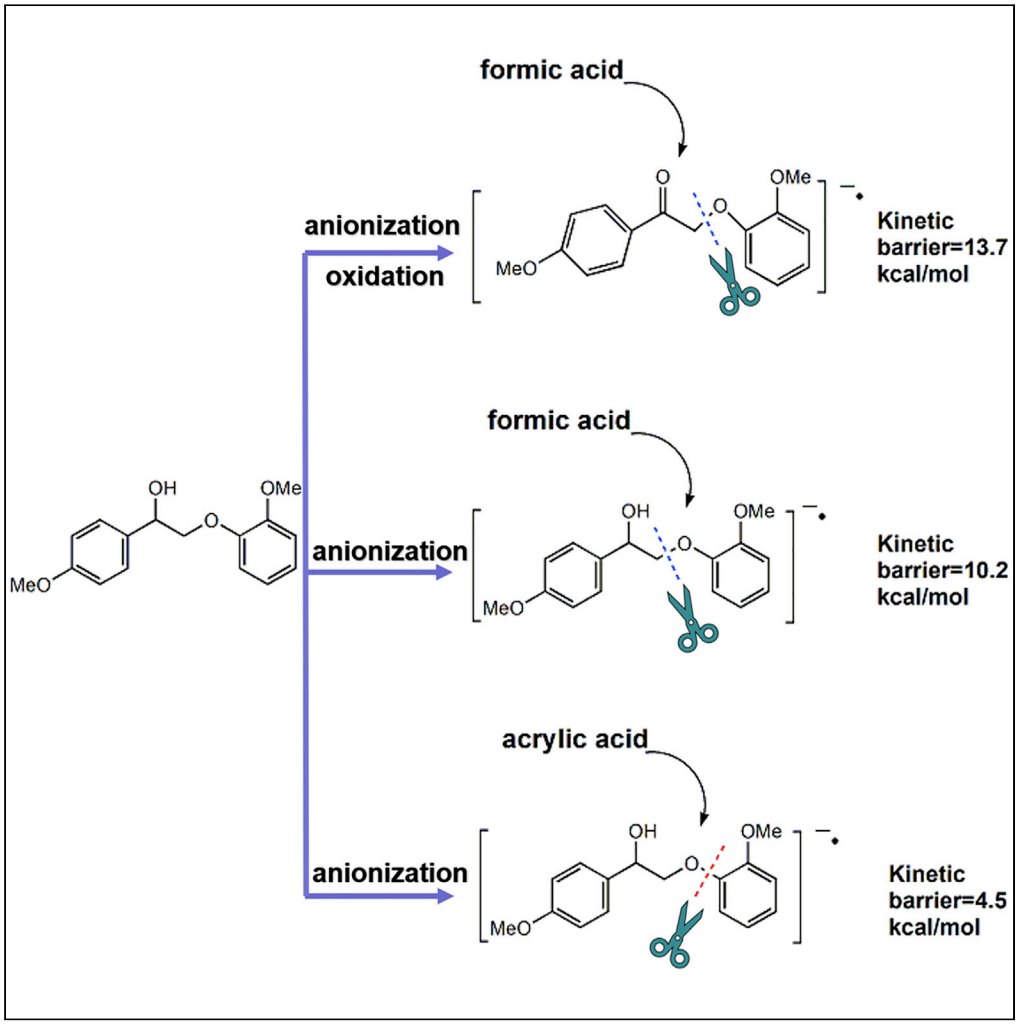

Zichen Wang, Mingtian Hao, Xiaoyu Li, Beibei Zhang, Mingyang Jiao, Bo-Zhen Chen

jiaomy@qibebt.ac.cn (M.J.)
bozhenchen@hotmail.com (B.-Z.C.)

Highlights

Lignin anion radicals without Cα oxidation can be degraded under mild conditions

The "double hydrogen bonds" structure is beneficial to lignin degradation

A promising and efficient lignin degradation versatile strategy is predicted

Wang et al., iScience 25, 103755
February 18, 2022
https://doi.org/10.1016/j.isci.2022.103755

iScience

CellPress
OPEN ACCESS

Article

Promising and efficient lignin degradation versatile strategy based on DFT calculations

Zichen Wang,[1] Mingtian Hao,[1] Xiaoyu Li,[1] Beibei Zhang,[1] Mingyang Jiao,[2,3,*] and Bo-Zhen Chen[1,4,*]

SUMMARY

The extraction of higher-value products from lignin degradations under mild conditions is a challenge. Previous research reported efficient two-step oxidation and reduction strategies for lignin degradation, which has great significance to lignin degradation. In this paper, the mechanism about the C-O bond cleavage of lignin with and without Cα oxidations has been studied systematically. Our calculation results show that the degradation of anionized lignin with Cα oxidations is kinetically and thermodynamically feasible. In addition, the calculations predict that the anionized lignin compounds without Cα oxidation also could be degraded under mild conditions. Moreover, we propose special lignin catalytic degradation systems containing the characteristic structure of "double hydrogen bonds." The double hydrogen bonds structure could further decrease the energy barriers of the C-O bond cleavage reaction. This provides a versatile strategy to design novel lignin degradation.

INTRODUCTION

The conversion of biomass into biofuels and biochemicals via environmentally friendly methods has provoked extensive attention due to the exhaustion of fossil fuel resources, the increasing worldwide energy demands, and the resultant negative environmental effects from fossil-fuel-based processes (Antonio Melero et al., 2012; Gallezot, 2012; Huber et al., 2006; Tuck et al., 2012). Compared with other renewable resources (solar, hydro, and wind power), only biomass is the organic carbon resource. Among biomass, lignin accounts for nearly 30% of the organic carbon sequestered in the biosphere, but it has not been utilized well nowadays (Wen et al., 2013). Lignin is a complex of phenolic polymers and rich in aromatic carbon (Chakar and Ragauskas, 2004; Hu et al., 2011; Ragauskas et al., 2006; Yue et al., 2012). Therefore, it can be used to produce liquid fuels and valuable chemicals such as low-molecular-weight aromatics. However, owing to its complex structure and stable bonds, lignin is resistant toward chemical degradation (Sergeev and Hartwig, 2011). The extraction of higher-value products from lignin is challenging. With the development of scientific understanding of lignin and the application of new catalysts, many new strategies of lignin degradation have been proposed. These current technologies can be generalized into acid/base catalyzed depolymerization (Dabral et al., 2018; Lindsay et al., 2019; Liu et al., 2019a; Nagel and Zhang, 2019; Zhu et al., 2018)/hydrolysis (Deuss et al., 2015; Nichols et al., 2010; Sedai et al., 2011; Sergeev et al., 2012), pyrolysis (Boerjan et al., 2003; Das et al., 2018; Kim et al., 2019; Li et al., 2018; Luo et al., 2019; Moon et al., 2018; Rinesch and Bolm, 2018; Zhang et al., 2018)/metal-catalyzed bond cleavage (Díaz-Urrutia et al., 2016; Gazi et al., 2015; Hanson et al., 2012; Jiang et al., 2016; Sedai et al., 2013)/photochemical lignin degradation (Ahmad et al., 2010; Bosque et al., 2017; Cao et al., 2018; Chen et al., 2017, 2020; Enright et al., 2019; Hao et al., 2018; Karkas et al., 2016; Li et al., 2019a, 2019b, 2020; Liu et al., 2019b; Luo et al., 2017a, 2017b; Nguyen et al., 2014, 2019; Srisasiwimon et al., 2018; Wu et al., 2018; Zhang, 2018; Zhou et al., 2018), and even biodegradation (Dabral et al., 2017; Ragauskas et al., 2014). Lignin degradation under acidic conditions is one of the most classical technologies. However, this method typically requires a temperature of at least 80°C. Moreover, the functional groups are not well tolerated and related environmental problems cannot be ignored. In 2014, Nguyen et al. reported efficient two-step oxidation and reduction strategies for lignin degradation (Nguyen et al., 2014). The first step is Cα oxidation and the second one is visible-light-induced anionization. The C-O bond cleavage could occur under mild conditions, obtaining an excellent yield. Most of the subsequent researches (Bosque et al., 2017; Wang et al., 2016; Zhang et al., 2017) extended the "two-step" cleavage strategy developed by Nguyen et al.

Taking the current energy shortages and environmental exacerbation into account, utilizing solar energy photocatalysis to obtain valuable products from lignin has been considered as a clean and energy-saving

[1]School of Chemical Sciences, University of Chinese Academy of Sciences, No. 19A, Yuquan Road, Beijing 100049, P. R. China

[2]Shandong Energy Institute, Qingdao 266101, Shandong, China

[3]Qingdao Institute of Bioenergy and Bioprocess Technology, Chinese Academy of Sciences, Qingdao 266101, Shandong, China

[4]Lead contact

*Correspondence: jiaomy@qibebt.ac.cn (M.J.), bozhenchen@hotmail.com (B.-Z.C.)

https://doi.org/10.1016/j.isci.2022.103755

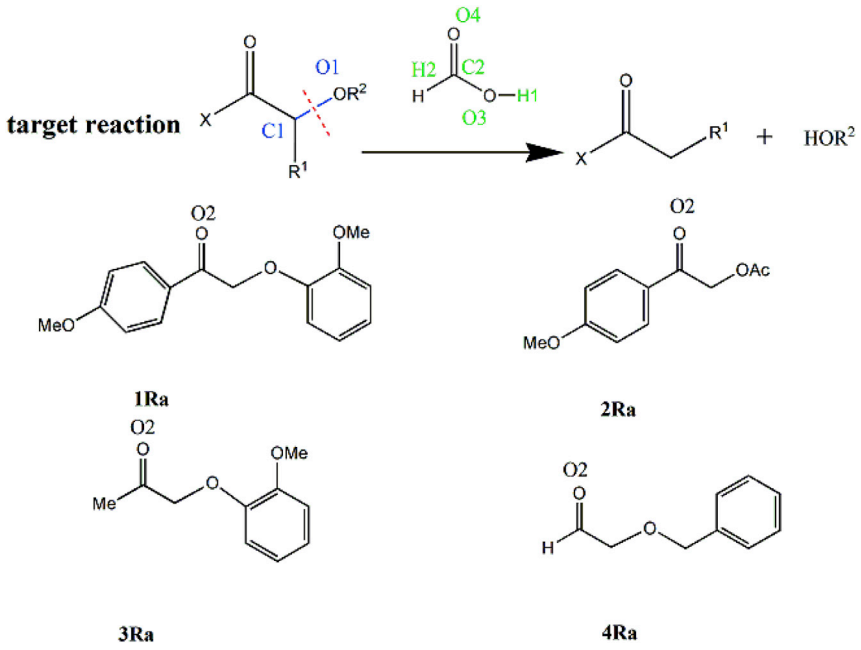

Scheme 1. The C-O cleavage of β-*O*-4 linkage in the lignin model compounds with Cα oxidations

method. However, the reaction mechanisms of the photocatalytic degradation of lignin are unclear. To the best of our knowledge, detailed computational studies on the classical two-step light-induced lignin degradation strategy have not been reported in the literature. Herein we attempt to elucidate the detailed mechanisms of the reactions of the photocatalytic lignin degradation. Our calculation results show that the two-step anionized lignin degradation strategy reported by Nguyen et al. is kinetically and thermodynamically feasible. Moreover, the results also predict that anionized lignin without Cα oxidations could also be degraded under mild conditions and that a characteristic structure of a double hydrogen bond (between the OH group on the Cα site and the carbonyl oxygen of the acrylic acid and between O atom of C-O bond of the β-*O*-4 linkage and the proton from acrylic acid) has significant effects on the C-O bond cleavage reaction. Our investigations can result in a clear process of degradation of lignin and provide important information for further designing novel lignin degradation strategy.

RESULTS AND DISCUSSION

The four molecules **1Ra**-**4Ra** (Scheme 1) were selected as model molecules of the lignin with Cα oxidation (the OH group of the α carbon is oxidized to C=O group). These four molecules have been used as lignin model compounds in experiment to explore a photochemical strategy for lignin degradation at room temperature, showing different degradation properties. Considering the reaction system includes formic acid in experiment (Nguyen et al., 2014), we calculated various possible lignin degradation processes with and without formic acid. For the convenience of description, we defined the C and O atoms from the C-O bond of the β-*O*-4 linkage and carbonyl oxygen in **1Ra**-**4Ra** as the C1, O1, and O2 atoms, respectively, and the hydroxy oxygen, carbonyl oxygen, hydroxy hydrogen, and hydrogen atom attached to carbonyl carbon in formic acid as the O3, O4, H1, and H2 atoms (Scheme 1).

The mechanism of C-O bond cleavage reaction for β-*O*-4 linkage

First, we calculated the reaction mechanism of the C-O bond cleavage of the β-*O*-4 linkage for the model molecule **1Ra** and its anionic radical **1Ra**$^{\cdot-}$. The free energy diagram with stretching of the C-O bond and the optimized structures of the key stationary points along the reaction pathways are shown in Figure 1. The C-O cleavage processes of the β-*O*-4 linkage for both **1Ra**$^{\cdot-}$ and **1Ra** consist of the two reaction steps: the formation of the intermediate (**1IM1** and **1IM***) via the transition state (**1TS1** and **1TS***) and the generation of the products (**1P** and **1P***). The free energy barrier for the radical anion **1Ra**$^{\cdot-}$ is predicted to be 8.4 kcal/mol, being 49.5 kcal/mol lower than that for the neutral state **1Ra**. Apparently, the radical anion is much more susceptible to degradation. By comparing the optimized structures of **1Ra**$^{\cdot-}$ and **1Ra**, we found

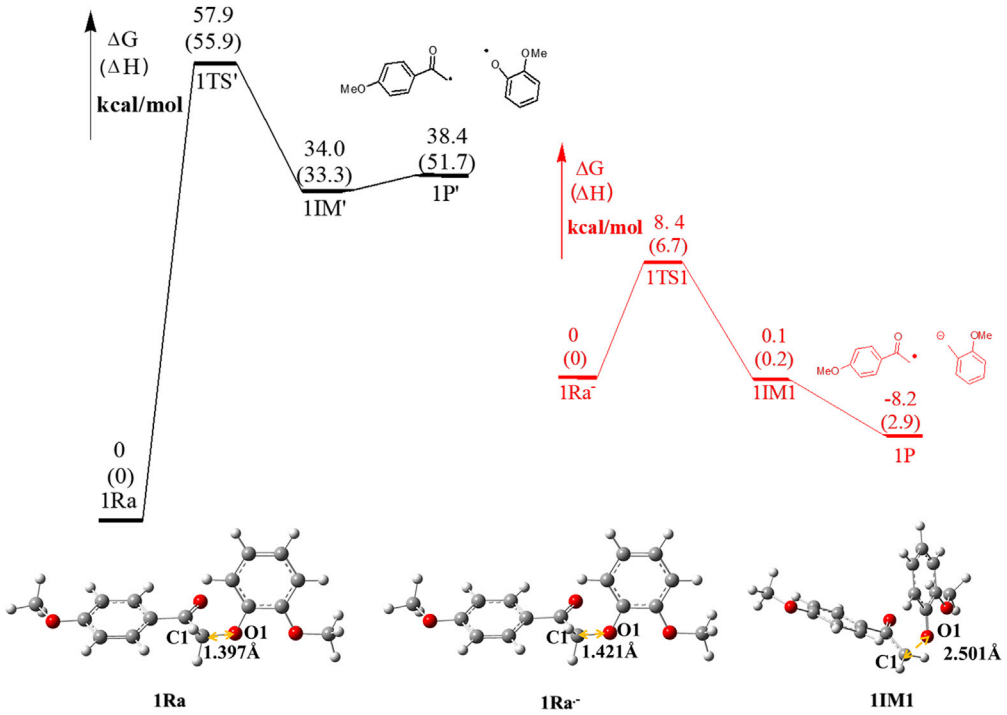

Figure 1. Schematic diagram of the free energy profile along the reaction pathways of the C-O cleavages of 1Ra and 1Ra$^{\cdot-}$, with enthalpies given in parentheses and optimized geometries of the key stationary points

that the distance between the C1 and O1 atoms (1.421 Å) in the former is significantly longer than that (1.397 Å) in the latter, indicating that the C1-O1 bond of the β-*O*-4 linkage is weakened in the radical anion (Figure 1). It is noted that the C1-O1 distance in **1IM1** is predicted to be 2.501 Å (Figure 1), implying that **1IM1** could separate into two fragments (*o*-methoxy phenol and methoxy acetophenone). In order to predict the charge and spin states for the two fragments, the charges and spin densities on the two moieties of **1IM1** were calculated and the results are shown in Table S1. It can be seen from Table S1 that the charge and spin density of the *o*-methoxy phenol are −0.74 and 0.22 e, respectively, which imply that the dissociation of **1IM1** should produce *o*-methoxy phenol anion and corresponding methoxy acetophenone radical. Furthermore, we performed the geometry optimization calculations for both the fragments and found that their geometry parameters are similar to those of **1IM1** (Figure S7). Therefore, the C-O cleavage of the β-*O*-4 linkage for **1Ra**$^{\cdot-}$ generates *o*-methoxy phenol anion and the corresponding methoxy acetophenone radical. The sum of free energy for the *o*-methoxy phenol anion and methoxy acetophenone radical relative to **1Ra**$^{\cdot-}$ is −8.2 kcal/mol. The lower free energy barrier and reaction free energy indicate that the C-O cleavage reaction of **1Ra**$^{\cdot-}$ is favorable both kinetically and thermodynamically in mild conditions.

The C-O bond cleavage of the neutral molecule **1Ra** leads to the formation of the *o*-methoxy phenol and methoxy acetophenone radicals by similar calculations to those for **1Ra**$^{\cdot-}$. The calculated free energy of the sum of the two radicals (**1P***) relative to **1Ra** is 38.4 kcal/mol. Comparing the free energy barriers and the reaction free energies of both the reactions, we conclude that, in the case of the lignin model molecule **1Ra**, the C-O cleavage in the radical anion is more favorable than that in the neutral molecule both kinetically and thermodynamically. Therefore, we only investigated the mechanism of the C-O cleavage for the radical anion of lignin model molecules in the following.

The calculated reaction pathways of the C-O bond cleavage for the radical anion of the model molecules **2Ra** and **4Ra** are similar to that of **1Ra** and the results are shown in Figure S1. Our calculations indicate that the overall free energy barriers (also corresponding to the barrier of the rate-determining step in the present work) of the **2Ra**$^{\cdot-}$ and **4Ra**$^{\cdot-}$ dissociations are 7.6 and 8.8 kcal/mol, respectively, which means that the two reactions are favorable kinetically. The calculated reaction free energies for the two reactions are −7.6 and 3.8 kcal/mol, respectively. It is worth noting that the optimized configuration structure of **3Ra**$^{\cdot-}$ is similar

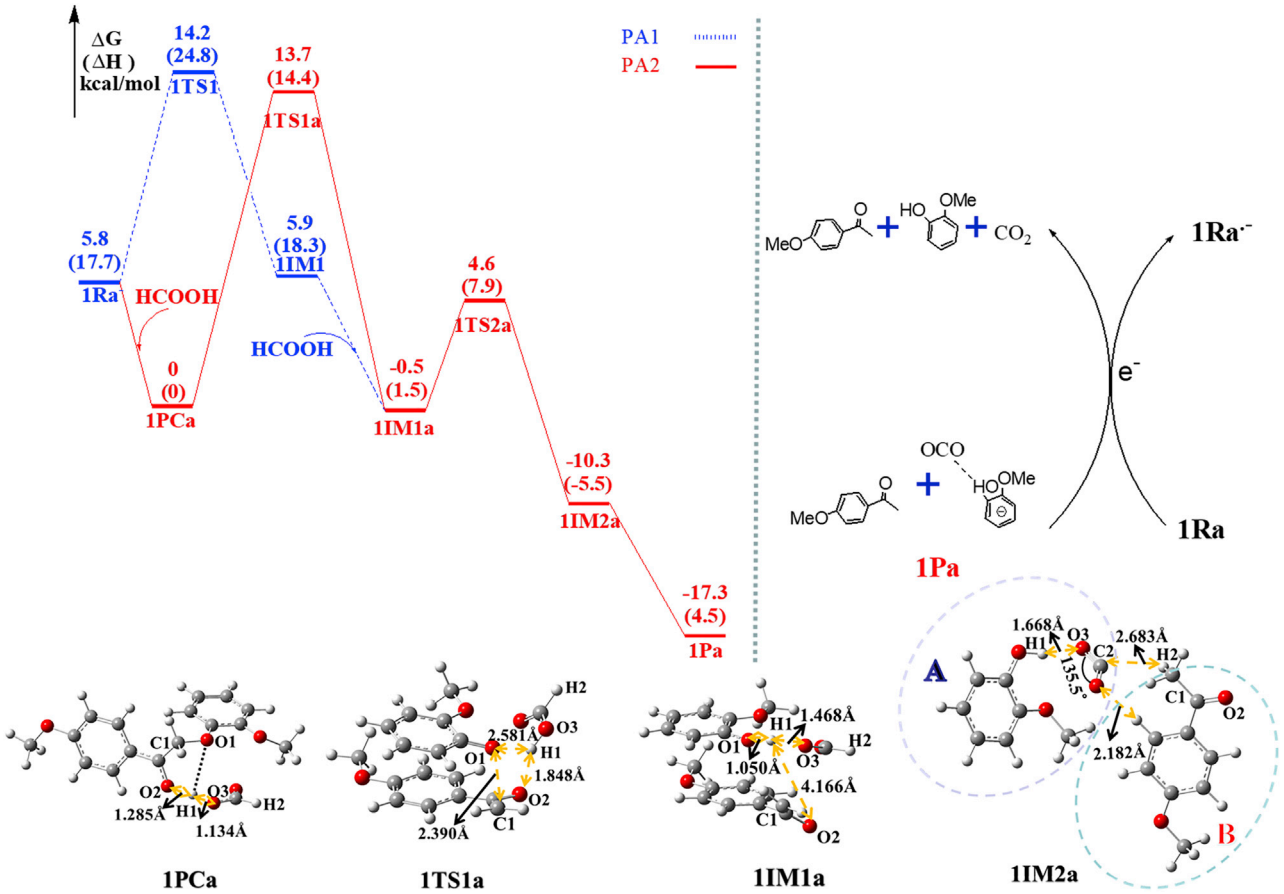

Figure 2. Schematic diagram of the free energy profile along the reaction pathways of PA1 (blue line) and PA2 (red line), with enthalpies given in parentheses and optimized structures of the key stationary points

to **1IM1**, **2IM1,** and **4IM1**. The C1-O1 bond length in **3Ra**$^{\cdot-}$ (3.213 Å) is significantly longer than that in neutral lignin molecule **3Ra** (1.409 Å). These results indicate that anionization could significantly weaken the C-O bond of the β-*O*-4 linkage, which allows this C-O bond cleavage under mild experimental conditions. Our calculation results that the C-O cleavage of lignin radical anion is kinetically and thermodynamically feasible support the experimental conclusions (Nguyen et al., 2014).

It is worth mentioning that, to generate the final product obtained experimentally, the *o*-methoxy phenol radical anion fragment needs to obtain a proton and the methoxy acetophenone radical fragment needs to further merge an H atom. Considering the degradation reaction was experimentally carried out in the presence of formic acid, we focus on the radical anion of lignin model molecules degradation process induced by formic acid in the following sections.

The mechanism of the C-O cleavage reaction for β-*O*-4 linkage induced by formic acid

The C-O bond cleavage reaction mechanisms of the anionic radical of lignin model molecules (**1Ra**$^{\cdot-}$-**4Ra**$^{\cdot-}$) in the presence of formic acid have been calculated. For **1Ra**$^{\cdot-}$, the two reaction pathways (**PA1** and **PA2**) were considered. Figure 2 shows the free energy diagram with stretching of the C-O bond, together with the optimized structures of the key stationary points along the two reaction pathways.

In the **PA1** pathway, lignin radical anions undergo the elongation of the C1-O1 bond first, generating the intermediate (**1IM1**), as described above. Subsequently, the alkoxy moiety of **1IM1** combines with a formic acid, forming **1IM1a**. The free energy barrier of the reaction along the **PA1** pathway is predicted to be 8.4 kcal/mol. In the **PA2** pathway, the **1Ra**$^{\cdot-}$ combines with a formic acid first, producing the pre-complex (**1PCa**). The free energy of the system decreases by 5.8 kcal/mol in this process. This is attributed to the

formation of hydrogen bond between the H1 and O2 atoms, which is reflected in the O2-H1 and O3-H1 distances being 1.285 and 1.134 Å, respectively, and the O2-H1-O3 angle being almost 180° in **1PCa**. Owing to excessive formic acid in the experiment, the **1PCa** is expected to be a more reasonable existence. After that, the C1-O1 bond stretches and the H1 atom migrates to the O1 atom of the β-*O*-4 linkage, forming the intermediate **1IM1a** through the transition state **1TS1a**. In **1TS1a**, the distances of O1-H1 and O2-H1 are 2.581 and 1.848 Å, respectively, which indicates that the O2 atom would compete with the O1 atom for the H1 atom. The free energy barrier of this reaction step is 13.7 kcal/mol. Comparing the **PA1** and **PA2** pathways, the formation of **1IM1a** is more possible in the **PA2** pathway. As shown in Figure 2, the O2-H1 distance increases to 4.166 Å in **1IM1a**, while the distance between the O1 and H1 atoms reduces to 1.050 Å, indicating that the H1 atom transfers from O2 to O1. Subsequently, the intermediate **1IM2a** is generated through the transition state **1TS2a**. The free energy barrier of this step is only 5.1 kcal/mol, which is significantly lower than that of the first reaction step. This suggests that the step from **1PCa** to **1IM1a** is the rate-determining step. Besides, the free energy of **1IM2a** is 9.8 kcal/mol lower than that of **1IM1a**. All these indicate that this reaction pathway is easy to carry out both kinetically and thermodynamically. It can be seen from Figure 2 that **1IM2a** consists of CO_2-containing *o*-methoxyphenol and *p*-methoxyacetophenone moieties and the shortest distance between the two moieties is predicted to be 2.182 Å. The charge and spin density of the CO_2-containing *o*-methoxyphenol moiety are calculated as −0.964 and 0.998 e, respectively (Table S1), indicating that the dissociation products of **1IM2a** should be the CO_2-containing *o*-methoxyphenol radical anion in the doublet state and *p*-methoxyacetophenone in the singlet state. These results are confirmed by the geometry optimization calculations for the two products (Figure S7). In order to ascertain the possibility of the CO_2-containing *o*-methoxyphenol radical anion transferring a single electron to **1Ra** to generate the final neutral product, we calculated the free energy changes (ΔG) of the following electron transfer reaction:

$$(CO_2 - containing\ o - methoxyphenol)^{\bullet -} + 1\mathrm{Ra} \rightarrow 1\mathrm{Ra}^{\bullet -} + CO_2 + o - methoxyphenol$$

The calculation results show that the change of free energies is −17.4 kcal/mol (see Table S2), which indicates that the reaction is thermodynamically feasible. Thus, CO_2, neutral *o*-methoxyphenol can be generated and a new **1Ra**$^{\cdot -}$ can be formed, realizing a cycle of electron transfer.

In summary, formic acid, as a hydrogen source, participates in the C-O bond cleavage reaction of the radical anion **1Ra**$^{\cdot -}$ by forming a relatively stable pre-complex (**1PCa**) with **1Ra**$^{\cdot -}$. The hydrogen bonding interaction between the carbonyl oxygen in **1Ra**$^{\cdot -}$ and the hydroxyl of formic acid is the main reason for the formation of **1PCa**. Subsequently, the hydroxy hydrogen of formic acid migrates from the carbonyl oxygen to the O atom of the C-O bond, and then the oxyacetophenone radical extracts H2 atom from formic acid to form **1IM2a**. At last, **1IM2a** dissociates into the CO_2-containing *o*-methoxyphenol radical anion and *p*-methoxyacetophenone. The former (CO_2-containing *o*-methoxyphenol radical anion) further gives an electron to the neutral lignin model molecule **1Ra**, producing **1Ra**$^{\cdot -}$, neutral *o*-methoxyphenol, and carbon dioxide. The feasibility of electron transfer from the CO_2-containing *o*-methoxyphenol radical anion to the neutral reactant achieves an electron transfer cycle.

We also studied the formic-acid-induced C-O bond cleavage process of β-*O*-4 linkages for the lignin model molecule radical anions **2Ra**$^{\cdot -}$-**4Ra**$^{\cdot -}$ and got a similar cleavage reaction mechanism. The detailed results can be seen in Figures S2–S4.

It is worth mentioning that the formic-acid-induced C-O cleavage reaction for **3Ra**$^{\cdot -}$ is somewhat different from the others. As shown in Figure 3, in the neutral lignin model molecule **3Ra**, the C1-O1 bond length is predicted to be 1.409 Å, whereas in its radical anion **3Ra**$^{\cdot -}$ to be 3.213 Å, indicating that the C1-O1 bond in **3Ra**$^{\cdot -}$ is obviously weakened. However, when **3Ra**$^{\cdot -}$ forms the pre-complex **3PCa** with formic acid, the activated C1-O1 bond in **3Ra**$^{\cdot -}$ is shortened to 1.432 Å. The structural characteristics of the C-O bond show significant differences in the stability for the C1-O1 bond: **3Ra** > **3PCa** > **3Ra**$^{\cdot -}$, which indicates that the hydrogen bond interaction between formic acid and carbonyl of **3Ra**$^{\cdot -}$ could be detrimental to the activation of the C1-O1 bond.

According to our calculations, the cleavage of the β-*O*-4 linkage in radical anion of lignin model molecules induced by formic acid includes two reaction steps. The first step is the hydrogen migration from hydroxyl hydrogen of the formic acid to alkoxy in lignin radical anions. The second step is Cα-radical abstracting another H atom of formic acid. The calculation result shows that the first step is the rate-determining step. In the first step, the carbonyl group, as an electron-withdrawing group, would compete with the O1 atom for interacting with the H1 atom and the hydrogen bond interaction between the O2 and H1

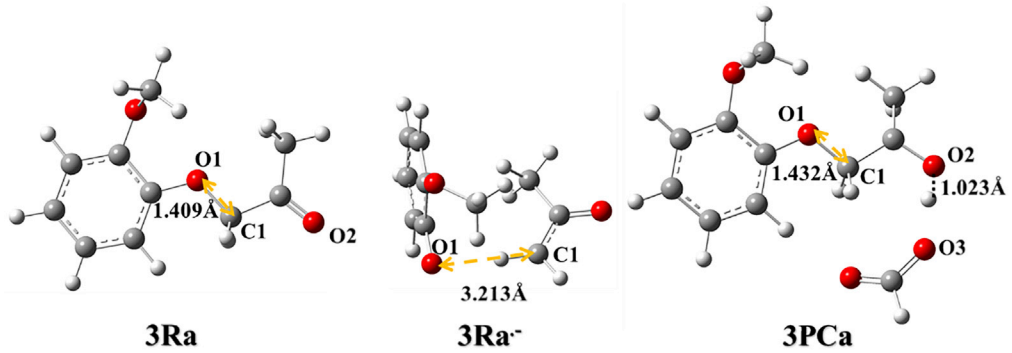

Figure 3. Optimized structures of 3Ra, 3Ra$^{\cdot-}$, and 3PCa

atoms might be unfavorable for the activation of the C1-O1 bond. It is reasonable to conclude that this interaction has negative effects on β-*O*-4 linkage cleavage.

The mechanism of the C-O cleavage reaction for the lignin model compounds without Cα oxidation

According to the above investigation, the selectively oxidized lignin has a negative effect on the reaction since its carboxyl oxygen is prone to interacting with the hydroxyl hydrogen of formic acid. We wondered whether the original lignin (without Cα oxidation) can also be degraded in the radical anion state. In order to gain insights into this query, we studied the degradation mechanism of four original lignin model molecules **1Rb**-**4Rb** (Scheme 2), which are the unselectively oxidized model molecules of **1Ra**-**4Ra** mentioned above, respectively.

The lignin model molecule radical anion **1Rb**$^{\cdot-}$ can also form a pre-complex **1PCb** with formic acid first. The free energy of **1PCb** is 3.4 kcal/mol lower than that of **1Rb**$^{\cdot-}$ and formic acid. The calculated free energy diagram along the C-O bond cleavage reaction path from **1PCb** can be seen in Figure 4. In contrast to the case of **1Ra**$^{\cdot-}$, the H1 atom is close to the O1 atom in the β-*O*-4 linkage (see notations in Scheme 2), and the distance between them is only 1.606 Å in **1PCb**.

With the splitting of the C1-O1 bond in **1PCb**, the intermediate **1IM1b** is formed via the transition state **1TS1b** with a free energy barrier of 10.2 kcal/mol. As shown in Figure 4, the O1-H1 distance is shortened to 1.031 Å and the C1-O1 distance increases to 3.420 Å in **1IM1b**. This indicates that the C1-O1 bond has greatly weakened. In addition, the O3 atom forms hydrogen bond with the H3 and H1 atoms (the angles of ∠O3-H1-O1 and ∠O2-H3-O3 are 168.0 and 167.3°, respectively, and the O3-H1 and O3-H3 distances are 1.510 and 1.673 Å, respectively). Owing to this hydrogen bond interaction, the free energy of **1IM1b** is greatly reduced. The free energy of **1IM1b** relative to **1PCb** is calculated to be −29.6 kcal/mol. These results fully demonstrate that the reaction step is favorable both kinetically and thermodynamically.

Subsequently, the H2 atom is transferred to the C1 atom, forming the intermediate **1IM2b** through the transition state **1TS2b** with a free energy barrier of 11.7 kcal/mol. In **1IM2b**, the C1-O1 distance is 5.064 Å, indicating that the C1-O1 bond has ruptured. As shown in Figure 4, **1IM2b** consists of two moieties: *o*-methoxyphenol and CO_2-containing *p*-methoxyphenylethanol. By calculating and analyzing the charge and spin density distributions of **1IM2b**, we conclude that the dissociation products (**1Pb**) from **1IM2b** should be the *o*-methoxyphenol neutral molecule, CO_2-containing *p*-methoxyphenylethanol radical anion (see Figure 4). The overall free energy barrier of the reaction from **1PCb** to **1Pb** is 10.2 kcal/mol, and the reaction free energy is −43.9 kcal/mol, indicating that the cleavage of the β-*O*-4 linkage of the original lignin model molecule radical anion **1Rb**$^{\cdot-}$ is favorable both kinetically and thermodynamically. Although **1Pb**$^{\cdot-}$ could not transfer a single electron to **1Rb** to complete its neutralization, the application of a constant positive potential or adding other electron acceptors could be a feasible alternative to neutralize **1Pb**$^{\cdot-}$, generating the final neutral product.

It is noted that the reaction free energy and the free energy barrier for the reaction from the precursor (**1PCb**) to the product (**1Pb**) are predicated to be 3.5 and 26.6 kcal/mol lower than those for the reaction from **1PCa** to **1Pa**, respectively. Therefore, the dissociation reaction of the C-O bond of the original lignin radical anion is more favorable than that of oxidized lignin radical anion and should be also feasible under mild conditions.

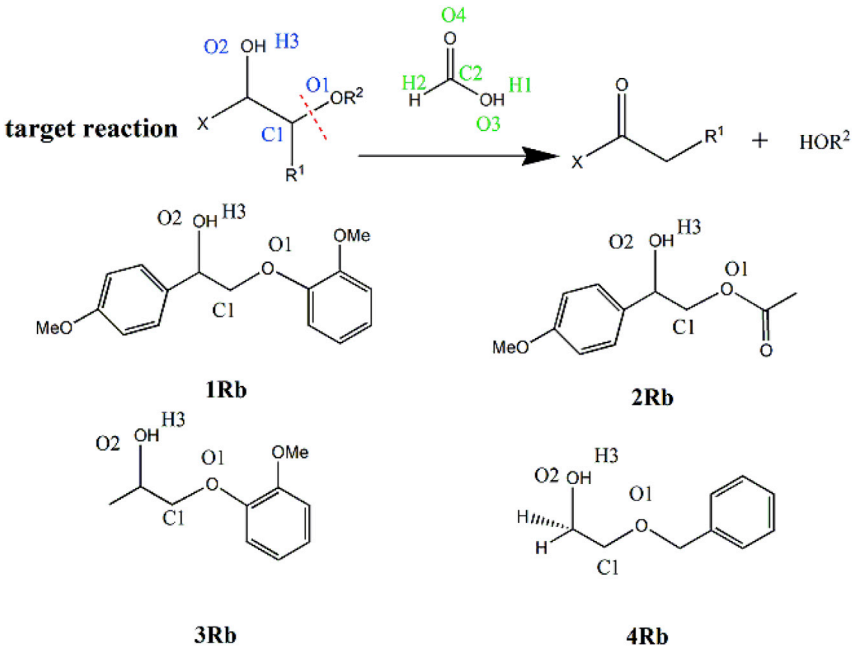

Scheme 2. The target reaction and the four selected lignin model molecules without Cα oxidation

The C-O bond cleavage mechanisms of **2Rb**$^{\cdot-}$ and **3Rb**$^{\cdot-}$ induced by formic acid are shown in Figure S4, which are similar to that of **1Rb**$^{\cdot-}$. However, the structure of **2PCb** is significantly different from those of **1PCb** and **3PCb**. This difference is due to the existence of another carbonyl group in **2Rb**$^{\cdot-}$. The calculated free energy barrier of the first step for **2PCb** is 14.6 kcal/mol, which is 4.4 and 8.4 kcal/mol higher than that for **1PCb** and **3PCb**, respectively. These results indicate that the presence of carbonyl group in the lignin could obstruct the breakage of the β-*O*-4 linkage.

For the lignin model molecule radical anion **4Rb**$^{\cdot-}$, we found different reaction processes. In the pre-complex **4PCb** (Figure 5), the C3-O1 bond is elongated to 3.307 Å not the C1-O1 bond discussed above. This indicates the dissociation products could be the CO_2-containing ethylene glycol and toluene. It should be noted that the ∠O2-H3-O4 and ∠O1-H1-O3 angles are predicted to be 170.6 and 176.5°, respectively, and the O4-H3 and O3-H1 distances are calculated to be 1.769 and 1.631 Å (Figure 5), illustrating the formation of double hydrogen bond between **4Rb**$^{\cdot-}$ and formic acid. This double hydrogen bond interaction greatly weakens the C3-O1 bond and also rationalizes that the free energy of **4PCb** is much lower than that of the reactants (**4Rb**$^{\cdot-}$ + formic acid). Then, the H2 atom bonds to C3 atom, forming the intermediate **4IM1b** via the transition state **4TS1b**. The free energy barrier of this reaction step is 13.2 kcal/mol (Figure 5), indicating that the reaction is favorable dynamically. In **4IM1b**, the C3-O1 distance is 6.127 Å, indicating the bond has ruptured. Thanks to the structure of the double hydrogen bond, the C-O bond cleavage site of lignin radical anion **4Rb**$^{\cdot-}$ changes from C1-O1 to C3-O1, which indicates that the existence of double hydrogen bonds could change the site of the C-O bond cleavage.

Owing to the absence of carbonyl groups in the **1PCb**, **3PCb,** and **4PCb** systems, the hydroxyl hydrogen of formic acid merely interacts with the O1 atom of the C-O bond, which reduces the free energy barrier of the first step of the C-O bond cleavage reaction.

The mechanism of the C-O bond cleavage reaction promoted by double hydrogen bonds

According to previous a study, the existence of the intramolecular hydrogen bonding interaction in lignin is unfavorable to the C-O bond cleavage (Kim et al., 2011), whereas we found that the hydrogen bond interaction between the OH group from lignin and the carbonyl oxygen of the carboxylic acid will remove the intramolecular hydrogen bonding interaction. Therefore, we hold the point that the double hydrogen bond structure could simultaneously eliminate the negative effects from carbonyl and intramolecular hydrogen bonds. As a consequence, it could decrease the free energy barrier of lignin degradation and change the

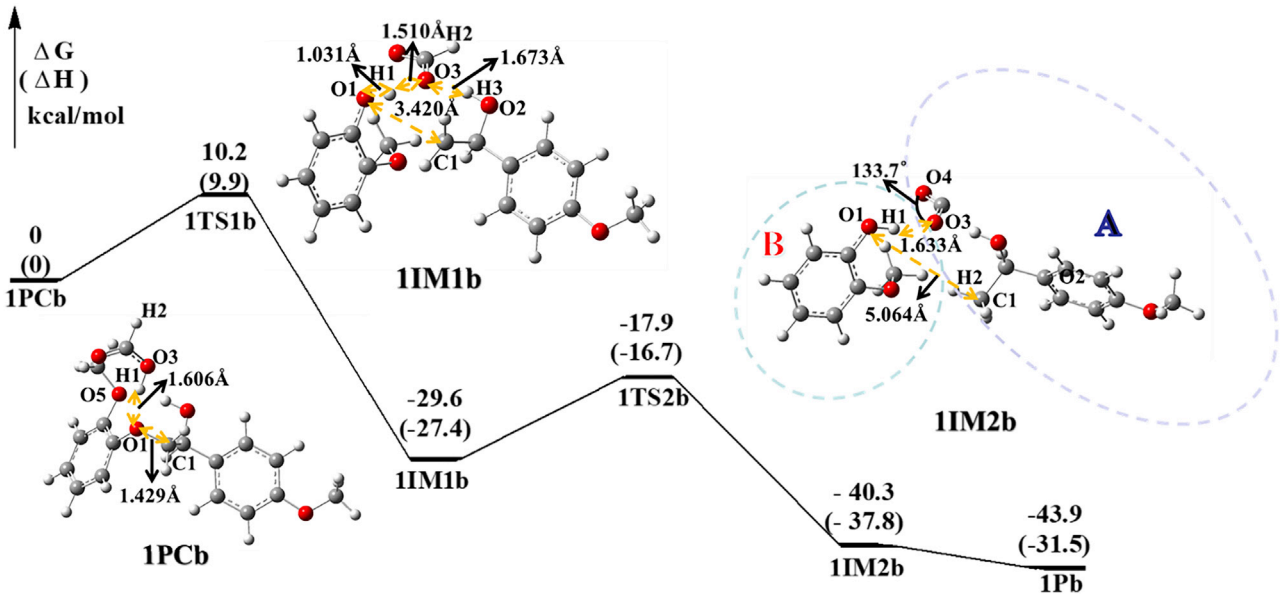

Figure 4. Schematic diagram of the free energy profile along the C-O bond cleavage reaction pathway of 1Rb$^{\cdot-}$, with enthalpies given in parentheses and optimized structures of the key stationary points

C-O bond cleavage site. Increasing the electronegativity of the carbonyl oxygen atom (O4 atom) of the carboxylic acid could enhance the formation of hydrogen bonds between O4 and H3, which is an indispensable condition for the double hydrogen bond structure generation.

Considering the O4 atom in acrylic acid with more electronegativity, we studied the C-O bond cleavage reaction of **1Rb**$^{\cdot-}$ and **3Rb**$^{\cdot-}$ lignin radical anions (structures shown in Scheme 2) induced by acrylic acid. Considering that the combination of the first intermediate and proton is easier in the following reaction step, we hold the point that the reaction step from the pre-complex to the first intermediate is vital. Therefore, this step was first considered in the following calculation.

Anionic lignin radical **1Rb**$^{\cdot-}$ could form the pre-complex (**1PCc**) with acrylic acid (see Figure 6) first. As expected, double hydrogen bonds are formed between **1Rb**$^{\cdot-}$ and acrylic acid in **1PCc**. It is reflected in the characteristic structure that the angles of ∠O1-H1-O3 and ∠O2-H3-O4 are 176.3° and 156.0°, whereas the O1-H1 and O4-H3 distances are 1.409 and 1.877 Å, respectively. Compared with **1PCb**, the H3-O5 distance in **1PCc** increases to 5.353 Å from 1.902 Å in **1PCb**, which shows that the formation of "double hydrogen bonds" destroys the intramolecular hydrogen bonding interaction as we expected. Moreover, the C3-O1 and C1-O1 distances in **1PCc** are 1.474 and 1.424 Å, respectively. The former is 0.07 Å longer than that in **1PCb,** whereas the latter is 0.05 Å shorter than that in **1PCb**. These indicate that the double hydrogen bonds tend to weaken the C3-O1 bond, not C1-O1 bond. Furthermore, we calculated the charge distribution of the pre-complexes **1PCb** and **1PCc**. The charge on the O4 atom in **1PCc** is −0.65 e, which is significantly more negative than that in **1PCb** (−0.48 e). This demonstrates that increasing the electronegativity on the carbonyl oxygen of the carboxylic acid could enhance the double hydrogen bond formation. With the C3-O1 bond being elongated, the **1PCc** passes through the transition state **1TSc** to form the intermediate **1IMc**. The free energy barrier and change of free energy for this reaction step are predicted to be 4.5 and −16.1 kcal/mol, respectively, indicating that the reaction from **1PCc** to **1IMc** is feasible both kinetically and thermodynamically. It is noted that the C3-O1 distance increases to 3.098 Å, whereas the C1-O1 distance is 1.402 Å in **1IMc**, suggesting that the characteristic structure of double hydrogen bonds leads to the C-O bond cleavage site change as we expected.

Similar to **1Rb**$^{\cdot-}$, **3Rb**$^{\cdot-}$ can also be combined with acrylic acid, producing the pre-complex (**3PCc**) with the double hydrogen bonds structure (Figure S5). The reaction step from **3PCc** to **3IMc** also has a lower free energy barrier and the C1-O3 bond is much longer than the C1-O1 bond in **3IMc**.

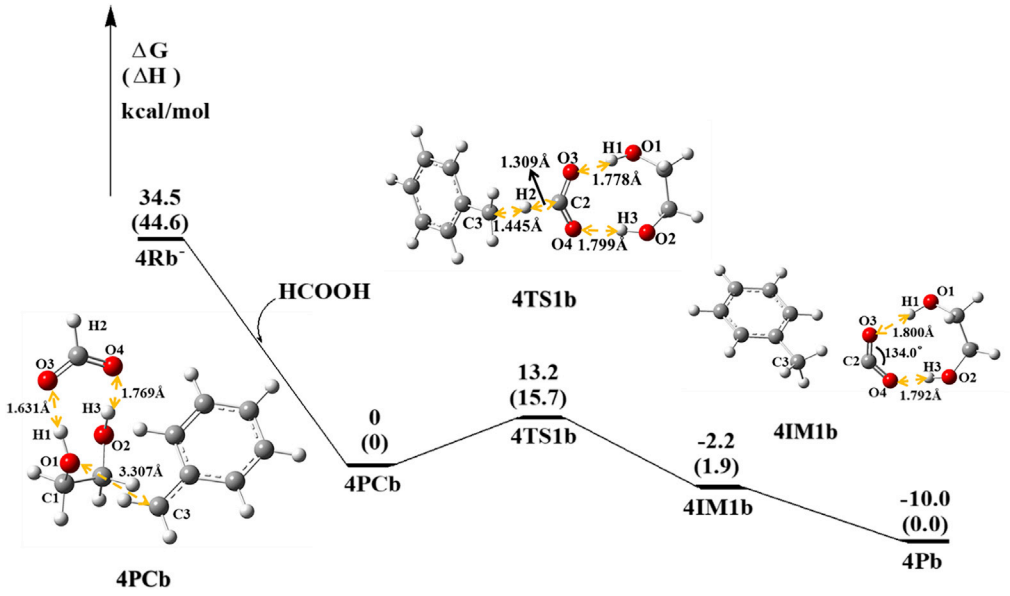

Figure 5. Schematic diagram of the free energy profile along the C-O bond cleavage reaction pathway of 4Rb$^{\cdot-}$, with enthalpies given in parentheses and optimized structures of the key stationary points

Furthermore, we calculated the C-O bond cleavage reaction of lignin radical anion **1Rb**$^{\cdot-}$ induced by acetic acid (Figure S6). Similar to the acrylic-acid-induced reaction process, the pre-complex (**1PCd**) with double hydrogen bonds is also formed between **1Rb**$^{\cdot-}$ and acetic acid. The free energy barrier from **1PCd** to an intermediate **1IMd** is lower than that of the corresponding step for **1PCb** and higher than that for **1PCc**. This result is consistent with the order of negative charge on the O4 atom in the pre-complex: **1PCb** < **1PCd** < **1PCc**. All the above facts just confirm that increasing the electronegativity on the carbonyl oxygen of the carboxylic acid could enhance the double hydrogen bond formation and thus promote the lignin degradation.

Considering that lignin models containing Cα-OH and Cγ-OH are more realistic model compounds as phenolic lignins, we took **5Ra** with Cα oxidation and **5Rb** without Cα oxidation (see Figure S8) as examples and calculated the C-O dissociation of their radical anions in the presence of formic acid. The calculated results are shown in Figure S8. The free energy barriers of C-O bond cleavage are predicted to be 8.3 kcal/mol for **5Ra**$^{\cdot-}$ and 5.5 kcal/mol for **5Rb**$^{\cdot-}$. The above results indicate that C-O bond rupture of **5Ra**$^{\cdot-}$ and **5Rb**$^{\cdot-}$ is kinetically feasible under mild conditions, similar to that of lignin models only containing Cα-OH. It is noted that the free energy barrier for **5Rb**$^{\cdot-}$ is significantly lower than that for **5Ra**$^{\cdot-}$. Our calculation results predicated that, in the absence of Cα oxidation, the anionic lignin compounds **5Rb** also could be degraded under mild conditions.

Conclusion

The degradation mechanisms of lignin model molecules with and without Cα oxidation have been investigated by the DFT M06-2X method. Our calculation results show that the C-O cleavage of lignin radical anion is feasible both kinetically and thermodynamically, supporting the experimental conclusions. Besides, the calculation results predict that the lignin radical anions without Cα oxidations could also be degraded under mild conditions. Moreover, the overall free energy barriers of the lignin radical anions without Cα oxidation are lower than that with the Cα oxidation.

Both intramolecular hydrogen bonds and carbonyl groups of lignin have negative effects on the cleavage reaction of the C-O bond for carboxylic-acid-induced lignin molecules. We designed special lignin catalytic degradation systems containing the characteristic structure with double hydrogen bonds. Furthermore, increasing the electronegativity on the carbonyl oxygen of the carboxylic acid could enhance the double hydrogen bond formation and thus promote the lignin degradation. Our work proposes potential lignin degradation strategy and could provide important ideas for further experimentally designing novel lignin degradation strategies.

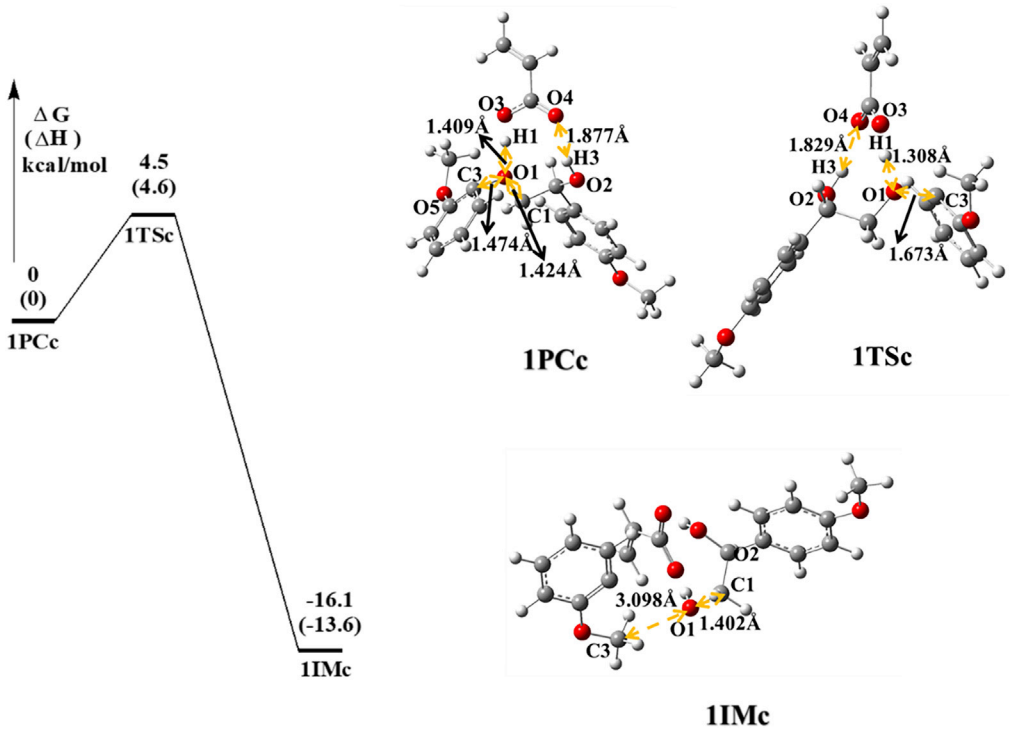

Figure 6. The relative free energies of stationary points along the C-O bond cleavage reaction pathway of 1Rb$^{\cdot-}$ induced by acrylic acid, with enthalpies given in parentheses and the structures of key stationary points

Limitations of the study

For current simulation of C-O bond cleavage reaction induced by the acrylic acid, the DFT method has its limitations in predicting the experimental products.

STAR★METHODS

Detailed methods are provided in the online version of this paper and include the following:

- KEY RESOURCES TABLE
- RESOURCE AVAILABILITY
  - Lead contact
  - Materials availability
  - Data and code availability
- METHOD DETAILS

SUPPLEMENTAL INFORMATION

Supplemental information can be found online at https://doi.org/10.1016/j.isci.2022.103755.

ACKNOWLEDGMENTS

We gratefully acknowledge the National Natural Science Foundation of China (No. 41530315) for supporting this work.

AUTHOR CONTRIBUTIONS

Z.W., M.J., and B.-Z.C. conceived the project; Z.W. and M.J. performed the DFT calculation; M.H., X.L., and B.Z. helped with the data analysis; Z.W., M.J., and B.-Z.C. wrote the manuscript.

DECLARATION OF INTERESTS

The authors declare no competing financial interest.

Received: May 19, 2021
Revised: December 14, 2021
Accepted: January 7, 2022
Published: February 18, 2022

REFERENCES

Ahmad, M., Taylor, C.R., Pink, D., Burton, K., Eastwood, D., Bending, G.D., and Bugg, T.D.H. (2010). Development of novel assays for lignin degradation: comparative analysis of bacterial and fungal lignin degraders. Mol. Biosyst. *6*, 815–821. https://doi.org/10.1039/b908966g.

Antonio Melero, J., Iglesias, J., and Garcia, A. (2012). Biomass as renewable feedstock in standard refinery units. Feasibility, opportunities and challenges. Energy Environ. Sci. *5*, 7393–7420. https://doi.org/10.1039/c2ee21231e.

Boerjan, W., Ralph, J., and Baucher, M. (2003). Lignin biosynthesis. Annu. Rev. Plant Biol. *54*, 519–546. https://doi.org/10.1146/annurev.arplant.54.031902.134938.

Bosque, I., Magallanes, G., Rigoulet, M., Karkas, M.D., and Stephenson, C.R.J. (2017). Redox catalysis facilitates lignin depolymerization. ACS Cent. Sci. *3*, 621–628. https://doi.org/10.1021/acscentsci.7b00140.

Cao, Y., Wang, N., He, X., Li, H.-R., and He, L.-N. (2018). Photocatalytic oxidation and subsequent hydrogenolysis of lignin β-O-4 models to aromatics promoted by in situ carbonic acid. ACS Sustain. Chem. Eng. *6*, 15032–15039. https://doi.org/10.1021/acssuschemeng.8b03498.

Chakar, F.S., and Ragauskas, A.J. (2004). Review of current and future softwood kraft lignin process chemistry. Industrial Crops and Products *20*, 131–141. https://doi.org/10.1016/j.indcrop.2004.04.016.

Chen, C., Liu, P., Xia, H., Zhou, M., Zhao, J., Sharma, B.K., and Jiang, J. (2020). Photocatalytic cleavage of beta-O-4 ether bonds in lignin over Ni/TiO2. Molecules *25*. https://doi.org/10.3390/molecules25092109.

Chen, J., Liu, W., Song, Z., Wang, H., and Xie, Y. (2017). Photocatalytic degradation of β-O-4 lignin model compound by In2S3 nanoparticles under visible light irradiation. Bioenergy Res. *11*, 166–173. https://doi.org/10.1007/s12155-017-9886-8.

Dabral, S., Engel, J., Mottweiler, J., Spoehrle, S.S.M., Lahive, C.W., and Bolm, C. (2018). Mechanistic studies of base-catalysed lignin depolymerisation in dimethyl carbonate. Green Chem. *20*, 170–182. https://doi.org/10.1039/c7gc03110f.

Dabral, S., Hernandez, J.G., Kamer, P.C.J., and Bolm, C. (2017). Organocatalytic chemoselective primary alcohol oxidation and subsequent cleavage of lignin model compounds and lignin. ChemSusChem *10*, 2707–2713. https://doi.org/10.1002/cssc.201700703.

Das, A., Rahimi, A., Ulbrich, A., Alherech, M., Motagamwala, A.H., Bhalla, A., da Costa Sousa, L., Balan, V., Dumesic, J.A., Hegg, E.L., et al. (2018). Lignin conversion to low-molecular-weight aromatics via an aerobic oxidation-hydrolysis sequence: comparison of different lignin sources. ACS Sustain. Chem. Eng. *6*, 3367–3374. https://doi.org/10.1021/acssuschemeng.7b03541.

Deuss, P.J., Scott, M., Tran, F., Westwood, N.J., de Vries, J.G., and Barta, K. (2015). Aromatic monomers by in situ conversion of reactive intermediates in the acid-catalyzed depolymerization of lignin. J. Am. Chem. Soc. *137*, 7456–7467. https://doi.org/10.1021/jacs.5b03693.

Díaz-Urrutia, C., Hurisso, B.B., Gauthier, P.M.P., Sedai, B., Singer, R.D., and Baker, R.T. (2016). Catalytic aerobic oxidation of lignin-derived bio-oils using oxovanadium and copper complex catalysts and ionic liquids. J. Mol. Catal. A Chem. *423*, 414–422. https://doi.org/10.1016/j.molcata.2016.07.035.

Enright, M.J., Gilbert-Bass, K., Sarsito, H., and Cossairt, B.M. (2019). Photolytic C–O bond cleavage with quantum dots. Chem. Mater. *31*, 2677–2682. https://doi.org/10.1021/acs.chemmater.9b00943.

Frisch, M.J., Trucks, G.W., Schlegel, H.B., Scuseria, G.E., Robb, M.A., Cheeseman, J.R., Zakrzewski, V.G., Montgomery, J.A., Stratmann, R.E., Burant, J.C., et al. (2009). Gaussian 09, G. I. Revision A. 1-SMP (Gaussian, Inc.).

Gallezot, P. (2012). Conversion of biomass to selected chemical products. Chem. Soc. Rev. *41*, 1538–1558. https://doi.org/10.1039/c1cs15147a.

Gazi, S., Ng, W.K.H., Ganguly, R., Moeljadi, A.M.P., Hirao, H., and Soo, H.S. (2015). Selective photocatalytic C-C bond cleavage under ambient conditions with earth abundant vanadium complexes. Chem. Sci. *6*, 7130–7142. https://doi.org/10.1039/c5sc02923f.

Hanson, S.K., Wu, R.L., and Silks, L.A. (2012). C-C or C-O bond cleavage in a phenolic lignin model compound: selectivity depends on vanadium catalyst. Angew. Chem. Int. Ed. Engl. *51*, 3410–3413. https://doi.org/10.1002/anie.201107020.

Hao, Z., Li, S., Sun, J., Li, S., and Zhang, F. (2018). Efficient visible-light-driven depolymerization of oxidized lignin to aromatics catalyzed by an iridium complex immobilized on mesocellular silica foams. Appl. Catal. B Environ. *237*, 366–372. https://doi.org/10.1016/j.apcatb.2018.05.072.

Hariharan, P.C., and Pople, J.A. (1973). The influence of polarization functions on molecular orbital hydrogenation energies. Theor. Chim. Acta *28*, 213–222. https://doi.org/10.1007/BF00533485.

Ho, J.M., Klamt, A., and Coote, M.L. (2010). Comment on the correct use of continuum solvent models. J. Phys. Chem. A *114*, 13442–13444. https://doi.org/10.1021/jp107136j.

Hu, L.H., Pan, H., Zhou, Y.H., and Zhang, M. (2011). Methods to improve lignin's reactivity as a phenol substitute and as replacement for other phenolic compounds: a brief review. Bioresources *6*, 3515–3525.

Huber, G.W., Iborra, S., and Corma, A. (2006). Synthesis of transportation fuels from biomass: chemistry, catalysts, and engineering. Chem. Rev. *106*, 4044–4098. https://doi.org/10.1021/cr068360d.

Jiang, Y.Y., Yan, L., Yu, H.Z., Zhang, Q., and Fu, Y. (2016). Mechanism of vanadium-catalyzed selective C-O and C-C cleavage of lignin model compound. ACS Catal. *6*, 4399–4410. https://doi.org/10.1021/acscatal.6b00239.

Karkas, M.D., Bosque, I., Matsuura, B.S., and Stephenson, C.R.J. (2016). Photocatalytic oxidation of lignin model systems by merging visible-light photoredox and palladium catalysis. Org. Lett. *18*, 5166–5169. https://doi.org/10.1021/acs.orglett.6b02651.

Kim, K.H., Jeong, K., Kim, S.-S., and Brown, R.C. (2019). Kinetic understanding of the effect of Na and Mg on pyrolytic behavior of lignin using a distributed activation energy model and density functional theory modeling. Green Chem. *21*, 1099–1107. https://doi.org/10.1039/c8gc02948b.

Kim, S., Chmely, S.C., Nimos, M.R., Bomble, Y.J., Foust, T.D., Paton, R.S., and Beckham, G.T. (2011). Computational study of bond dissociation enthalpies for a large range of native and modified lignins. J. Phys. Chem. Lett. *2*, 2846–2852. https://doi.org/10.1021/jz201182w.

Li, J., Sun, H., Liu, J.-X., Zhang, J.-J., Li, Z.-X., and Fu, Y. (2018). Selective reductive cleavage of C O bond in lignin model compounds over nitrogen-doped carbon-supported iron catalysts. Mol. Catal. *452*, 36–45. https://doi.org/10.1016/j.mcat.2018.03.014.

Li, H., Bunrit, A., Lu, J., Gao, Z., Luo, N., Liu, H., and Wang, F. (2019a). Photocatalytic cleavage of aryl ether in modified lignin to non-phenolic aromatics. ACS Catal. *9*, 8843–8851. https://doi.org/10.1021/acscatal.9b02719.

Li, S., Li, Z.-J., Yu, H., Sytu, M.R., Wang, Y., Beeri, D., Zheng, W., Sherman, B.D., Yoo, C.G., and Leem, G. (2019b). Solar-driven lignin oxidation via hydrogen atom transfer with a dye-sensitized TiO2 photoanode. ACS Energy Lett. *5*, 777–784. https://doi.org/10.1021/acsenergylett.9b02391.

Li, T., Mo, J.Y., Weekes, D.M., Dettelbach, K.E., Jansonius, R.P., Sammis, G.M., and Berlinguette, C.P. (2020). Photoelectrochemical decomposition of lignin model compound on a BiVO4 photoanode. ChemSusChem *13*, 3622–3626. https://doi.org/10.1002/cssc.202001134.

Lindsay, A.C., Kudo, S., and Sperry, J. (2019). Cleavage of lignin model compounds and lignin(ox) using aqueous oxalic acid. Org. Biomol.

Chem. *17*, 7408–7415. https://doi.org/10.1039/c9ob01452g.

Liu, H., Zhu, L., Wallraf, A.-M., Räuber, C., Grande, P.M., Anders, N., Gertler, C., Werner, B., Klankermayer, J., Leitner, W., and Schwaneberg, U. (2019a). Depolymerization of laccase-oxidized lignin in aqueous alkaline solution at 37°C. ACS Sustain. Chem. Eng. *7*, 11150–11156. https://doi.org/10.1021/acssuschemeng.9b00204.

Liu, X., Duan, X., Wei, W., Wang, S., and Ni, B.-J. (2019b). Photocatalytic conversion of lignocellulosic biomass to valuable products. Green Chem. *21*, 4266–4289. https://doi.org/10.1039/c9gc01728c.

Luo, J., Zhang, X., Lu, J., and Zhang, J. (2017a). Fine tuning the redox potentials of carbazolic porous organic frameworks for visible-light photoredox catalytic degradation of lignin β-O-4 models. ACS Catal. *7*, 5062–5070. https://doi.org/10.1021/acscatal.7b01010.

Luo, N., Wang, M., Li, H., Zhang, J., Hou, T., Chen, H., Zhang, X., Lu, J., and Wang, F. (2017b). Visible-light-driven self-hydrogen transfer hydrogenolysis of lignin models and extracts into phenolic products. ACS Catal. *7*, 4571–4580. https://doi.org/10.1021/acscatal.7b01043.

Luo, Z., Lu, K., Yang, Y., Li, S., and Li, G. (2019). Catalytic fast pyrolysis of lignin to produce aromatic hydrocarbons: optimal conditions and reaction mechanism. RSC Adv. *9*, 31960–31968. https://doi.org/10.1039/c9ra02538c.

Marenich, A.V., Cramer, C.J., and Truhlar, D.G. (2009a). Performance of SM6, SM8, and SMD on the SAMPL1 test set for the prediction of small-molecule solvation free energies. J. Phys. Chem. B *113*, 4538–4543. https://doi.org/10.1021/jp809094y.

Marenich, A.V., Cramer, C.J., and Truhlar, D.G. (2009b). Universal solvation model based on solute electron density and on a continuum model of the solvent defined by the bulk dielectric constant and atomic surface tensions. J. Phys. Chem. B *113*, 6378–6396. https://doi.org/10.1021/jp810292n.

Moon, S., Lee, Y., Choi, S., Hong, S., Lee, S., Park, A.-H.A., and Park, Y. (2018). Spectroscopic investigation of thermochemical depolymerization of lignin model compounds in the presence of novel liquidlike nanoparticle organic hybrid solvents for efficient biomass valorization. Org. Process Res. Dev. *22*, 1723–1732. https://doi.org/10.1021/acs.oprd.8b00282.

Nagel, E., and Zhang, C. (2019). Hydrothermal decomposition of a lignin dimer under neutral and basic conditions: a mechanism study. Ind. Eng. Chem. Res. *58*, 18866–18880. https://doi.org/10.1021/acs.iecr.9b00400.

Nguyen, J.D., Matsuura, B.S., and Stephenson, C.R.J. (2014). A photochemical strategy for lignin degradation at room temperature. J. Am. Chem. Soc. *136*, 1218–1221. https://doi.org/10.1021/ja4113462.

Nguyen, S.T., Murray, P.R.D., and Knowles, R.R. (2019). Light-driven depolymerization of native lignin enabled by proton-coupled electron transfer. ACS Catal. *10*, 800–805. https://doi.org/10.1021/acscatal.9b04813.

Nichols, J.M., Bishop, L.M., Bergman, R.G., and Ellman, J.A. (2010). Catalytic C-O bond cleavage of 2-aryloxy-1-arylethanols and its application to the depolymerization of lignin-related polymers. J. Am. Chem. Soc. *132*, 12554–12555. https://doi.org/10.1021/ja106101f.

Ragauskas, A.J., Beckham, G.T., Biddy, M.J., Chandra, R., Chen, F., Davis, M.F., Davison, B.H., Dixon, R.A., Gilna, P., Keller, M., et al. (2014). Lignin valorization: improving lignin processing in the biorefinery. Science *344*, 1246843. https://doi.org/10.1126/science.1246843.

Ragauskas, A.J., Williams, C.K., Davison, B.H., Britovsek, G., Cairney, J., Eckert, C.A., Frederick, W.J., Hallett, J.P., Leak, D.J., Liotta, C.L., et al. (2006). The path forward for biofuels and biomaterials. Science *311*, 484–489. https://doi.org/10.1126/science.1114736.

Rinesch, T., and Bolm, C. (2018). Cobalt-catalyzed oxidation of the β-O-4 bond in lignin and lignin model compounds. ACS Omega *3*, 8386–8392. https://doi.org/10.1021/acsomega.8b00994.

Sedai, B., Diaz-Urrutia, C., Baker, R.T., Wu, R.L., Silks, L.A., and Hanson, S.K. (2011). Comparison of copper and vanadium homogeneous catalysts for aerobic oxidation of lignin models. ACS Catal. *1*, 794–804. https://doi.org/10.1021/cs200149v.

Sedai, B., Diaz-Urrutia, C., Baker, R.T., Wu, R.L., Silks, L.A., and Hanson, S.K. (2013). Aerobic oxidation of beta-1 lignin model compounds with copper and oxovanadium catalysts. ACS Catal. *3*, 3111–3122. https://doi.org/10.1021/cs400636k.

Sergeev, A.G., and Hartwig, J.F. (2011). Selective, nickel-catalyzed hydrogenolysis of aryl ethers. Science *332*, 1263.

Sergeev, A.G., Webb, J.D., and Hartwig, J.F. (2012). A heterogeneous nickel catalyst for the hydrogenolysis of aryl ethers without arene hydrogenation. J. Am. Chem. Soc. *134*, 20226–20229. https://doi.org/10.1021/ja3085912.

Srisasiwimon, N., Chuangchote, S., Laosiripojana, N., and Sagawa, T. (2018). TiO2/lignin-based carbon composited photocatalysts for enhanced photocatalytic conversion of lignin to high value chemicals. ACS Sustain. Chem. Eng. *6*, 13968–13976. https://doi.org/10.1021/acssuschemeng.8b02353.

Stephens, P.J., Devlin, F.J., Chabalowski, C.F., and Frisch, M.J. (1994). Ab-initio calculation of vibrational absorption and circular-dichroism spectra using density-functional force-fields. J. Phys. Chem. *98*, 11623–11627. https://doi.org/10.1021/j100096a001.

Tuck, C.O., Perez, E., Horvath, I.T., Sheldon, R.A., and Poliakoff, M. (2012). Valorization of biomass: deriving more value from waste. Science *337*, 695–699. https://doi.org/10.1126/science.1218930.

Wang, M., Lu, J., Zhang, X., Li, L., Li, H., Luo, N., and Wang, F. (2016). Two-step, catalytic C–C bond oxidative cleavage process converts lignin models and extracts to aromatic acids. ACS Catal. *6*, 6086–6090. https://doi.org/10.1021/acscatal.6b02049.

Wen, J.L., Xue, B.L., Xu, F., Sun, R.C., and Pinkert, A. (2013). Unmasking the structural features and property of lignin from bamboo. Ind. Crops Prod. *42*, 332–343. https://doi.org/10.1016/j.indcrop.2012.05.041.

Wu, X., Fan, X., Xie, S., Lin, J., Cheng, J., Zhang, Q., Chen, L., and Wang, Y. (2018). Solar energy-driven lignin-first approach to full utilization of lignocellulosic biomass under mild conditions. Nat. Catal. *1*, 772–780. https://doi.org/10.1038/s41929-018-0148-8.

Yue, F.X., Lu, F.C., Sun, R.C., and Ralph, J. (2012). Synthesis and characterization of new 5-linked pinoresinol lignin models. Chem. Eur. J. *18*, 16402–16410. https://doi.org/10.1002/chem.201201506.

Zhang, C.F., Li, H.J., Lu, J.M., Zhang, X.C., MacArthur, K.E., Heggen, M., and Wang, F. (2017). Promoting lignin depolymerization and restraining the condensation via an oxidation-hydrogenation strategy. ACS Catal. *7*, 3419–3429. https://doi.org/10.1021/acscatal.7b00148.

Zhang, J. (2018). Conversion of lignin models by photoredox catalysis. ChemSusChem *11*, 3071–3080. https://doi.org/10.1002/cssc.201801370.

Zhang, J., Lombardo, L., Gözaydın, G., Dyson, P.J., and Yan, N. (2018). Single-step conversion of lignin monomers to phenol: bridging the gap between lignin and high-value chemicals. Chin. J. Catal. *39*, 1445–1452. https://doi.org/10.1016/s1872-2067(18)63132-8.

Zhou, W., Nakahashi, J., Miura, T., and Murakami, M. (2018). Light/copper relay for aerobic fragmentation of lignin model compounds. Asian J. Org. Chem. *7*, 2431–2434. https://doi.org/10.1002/ajoc.201800520.

Zhu, Y., Han, Z., Fu, L., Liu, C., and Zhang, D. (2018). Cleavage of the beta-O-4 bond in a lignin model compound using the acidic ionic liquid 1-H-3-methylimidazolium chloride as catalyst: a DFT mechanistic study. J. Mol. Model. *24*, 322. https://doi.org/10.1007/s00894-018-3854-x.

STAR★METHODS

KEY RESOURCES TABLE

REAGENT or RESOURCE	SOURCE	IDENTIFIER
Software and algorithms		
Gaussian 09	Frisch et al., 2009	RRID:SCR_014897; https://gaussian.com

RESOURCE AVAILABILITY

Lead contact

Further information and requests for resources should be directed to and will be fulfilled by the lead contact, Bo-Zhen Chen (bozhenchen@hotmail.com).

Materials availability

This study did not generate new unique reagents.

Data and code availability

- The published article includes all datasets generated or analyzed during this study.
- This study did not generate new code.
- Any additional information required to reanalyze the data reported in this paper is available from the lead contact upon request.

METHOD DETAILS

The geometries of all the stationary points along the reaction pathways, including the reactants, intermediates, transition states, and products, were optimized using the DFT (Stephens et al., 1994) M06-2X (Marenich et al., 2009b) method in conjunction with the 6-31+G(d,p) basis set (Hariharan and Pople, 1973). Harmonic vibrational frequency analysis calculations at the M06-2X/6-31+G(d,p) level at 298 K were performed to confirm each stationary point to be either a minimum (no imaginary frequencies) or a transition-state (only one imaginary frequency) and to obtain its zero-point energies and thermal correction data. The intrinsic reaction coordinate (IRC) pathways have been traced to confirm whether the transition state connects the reactant, intermediate or product, and to verify the critical reaction steps involved in our proposed mechanisms. Gibbs free energies and enthalpies in gas phase at 298 K and 1 atm were calculated at the same level. The single-point solvation Gibbs free energies were calculated by using SMD solvation model (Ho et al., 2010; Marenich et al., 2009a) in acetonitrile solvent (used in experiment) at the M06-2X/6-311+G(d,p) level. The natural bond orbital (NBO) analyses at the M06-2X/6-31+G(d,p) level were applied to characterize the electronic structure of some species.

Gibbs free energies and enthalpies in the solvent phase at 298 K and 1 atm are used in the following discussion, unless otherwise specified, and the enthalpies are also given. All of the quantum chemical calculations were performed using the Gaussian 09 program (Frisch et al., 2009).